Research on Engineering Structures & Materials
www.jresm.org
Research Group

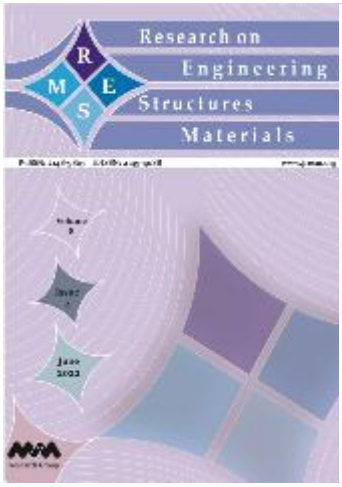

Characterization and predictive modeling of thermally aged glass fiber reinforced plastic composites

Md Mijanur Rahman, M Muzibur Rahman

Online Publication Date: 10 November 2023
URL: http://www.jresm.org/archive/resm2023.24me0609rs.html
DOI: http://dx.doi.org/10.17515/resm2023.24me0609rs
Journal Abbreviation: *Res. Eng. Struct. Mater.*

To cite this article
Rahman Md M, Rahman MM. Characterization and predictive modeling of thermally aged glass fiber reinforced plastic composites. *Res. Eng. Struct. Mater.*, 2024; 10(1): 305-330.

Research on Engineering Structures & Materials
www.jresm.org
Research Group

Research Article

Characterization and predictive modeling of thermally aged glass fiber reinforced plastic composites

Md Mijanur Rahman*[1,a], M Muzibur Rahman[2,b]

[1]*Department of Mechanical and Aerospace Engineering, Oklahoma State University, U.S.A*
[2]*Department of Mechanical Engineering, Sonargaon University, Bangladesh*

Article Info

Article history:

Received 09 June 2023
Accepted 05 Nov 2023

Keywords:

Glass fiber reinforced plastic composite; Thermal aging; Material characterization; Predictive modeling; Artificial neural network

Abstract

Glass fiber reinforced plastics (GFRP) are exposed to thermal aging in their widespread aerospace applications. Evaluating the effect of mechanical properties due to thermal aging has remained a challenge. An experimental investigation to characterize the thermal aging effects of glass fiber epoxy composites as well as the development of a predictive modeling is presented here. Tensile test samples have been thermally aged at 50°C, 100°C, 150°C and 200°C for 30 mins, 60 mins, 90 mins and 120 mins. At higher temperatures, the samples have shown a gradually increasing brown color while emitting a burning smell. The tensile test shows that the UTS value decreases as the thermal aging temperature increases. The predictive model has been prepared by combining image processing, regression analysis and two cascaded artificial neural networks (ANNs). The model reads the photographic image of the sample and uses the color change as an identifier. Cascaded ANNs estimate the thermal aging temperature and time from the image processing program. Finally, the ANN's output is forwarded to the developed regression equation to get the estimated UTS. The predictive model's estimated UTS shows an average accuracy of 97% when compared to the experimental results.

1. Introduction

Glass fiber-reinforced plastic (GFRP) composites have seen widespread applications in the Aerospace industry [1]. In aerospace applications, GFRP composites are subjected to thermal aging at elevated temperatures, especially in UAV operations, aircraft fuselage panels, aircraft wingtips, control surfaces, bleed air ducts and inlet fan blade casing [2]. In these aerospace components, the mechanical properties of GFRP is very important to ensure safe operation during flight. The mechanical behavior of a fiber-reinforced composite basically depends on the fiber strength and modulus, the chemical stability, matrix strength and the interface bonding between the fiber/matrix to enable stress transfer [3]. Scientists and engineers are well aware of the properties of fiber reinforced polymers, but there are still a lot of questions concerning their durability and performance under harsh environmental conditions.[4].

A considerable amount of literature has been published regarding the thermal aging of GFRPs and its influence on mechanical properties. Bazli et al. [5] investigated the behavior of unidirectional, woven and chopped strand GFRP laminates subjected to impact and flexure loads at extreme temperatures. According to the findings, GFRP laminates' flexural and impact capabilities generally deteriorate as exposure time and temperature rise, and as laminate thickness decreases. Kun et al. [6] developed an epoxy glass fiber composite and performed wet and heat cycle aging tests. They found that the composites' mechanical

*Corresponding author: mdmirah@okstate.edu
[a] https://orcid.org/0000-0001-9734-0279; [b] https://orcid.org/0000-0002-7444-9009
DOI: http://dx.doi.org/10.17515/resm2023.24me0609rs

and dielectric properties deteriorated over time. Zuo et al. [7] performed an experiment in which the isothermal and non-isothermal crystallization behaviors of glass fiber-reinforced polyphenylene sulfide were rigorously investigated and a broad variety of widely used models were applied to this material. It was discovered that the polymer crystallizes more slowly during crystallization when it has undergone extreme age and degeneration. According to Birger et al. [8], thermal aging influences the mechanical characteristics and failure processes of graphite-fabric epoxy composites exposed to flexural stress. The authors thermally aged the samples at 170 °C for 120, 240, and 626 hours. For the longest exposure period, bare fibers were detectable due to the weakening of the fiber-matrix interface, and as thermal aging progresses, fracture transforms from ductile with more plastic deformations to brittle. Mouritz et al. [9] investigated the post-fire residual flexure strength of glass, carbon, and Kevlar-reinforced polyester, epoxy, and phenolic-based laminates. They discovered that even a little amount of fire damage resulted in a significant decrease in strength qualities, and the model used to forecast the strength properties showed a strong connection with the experimental data. Dodds et al. [10] subjected the epoxy, phenolic, and polyester GFRP panels to a high-temperature fire and compared the behavior using thermal modeling. Phenolic-based GFRP laminates were shown to be more susceptible to delamination. In addition, the thickness of the composites had a significant effect in their fire resistance.

Several researchers have also noted the color changes due to thermal aging. Zhenbo Lan et al. [11] studied the color changes and mechanical properties of glass fiber-reinforced polycarbonate (GF-PC) composites after aging at various temperatures. The experiment revealed that the brightness of the GF-PC composite is related to trends detected in their tensile strength and bending strength. Song et al. [12] investigated the impact of thermal aging on the mechanical properties of glass-reinforced PEI plate composites. They found that as the aging temperature increased from 80 to 145 C, both the tensile and flexural strengths of the GF/PEI composite samples dropped, which was also reflected in their color difference.

The glass transition temperature (Tg) is an important consideration for the thermal aging study of all FRPs. As such, several researchers have studied the effect of thermal aging at temperatures near Tg. In a study relevant to ours, Zavatta et al. [13] conducted research to determine how the strength of carbon fabric/epoxy composites changed as a result of thermal aging in air. For aging at temperatures below the glass transition temperature (Tg) of the resin, a considerable decline in strength was observed. In contrast, a fast drop in strength was found at aging temperatures exceeding Tg. Furthermore, it was determined that even brief exposure to operating temperatures over Tg might significantly reduce the load-bearing capacity of CFRP components.

For developing predictive models, researchers have also experimented with using various techniques. Gibson et al. [14] studied the raised temperature effect on the mechanical properties of woven glass fiber/polypropylene composites and suggested a 3-parameter model to define the tensile behavior and a 2-parameter model to define the compressive behavior to analyze the effects. Kim et al.[15] experimented with multiple regression analysis (MRA) and polynomial regression analysis (PRA) and ANNs, to analyze the factors affecting the tensile strength of basalt and glass fiber-reinforced polymers (FRPs). They found that ANNs could be the most efficient model for forecasting the durability of FRPs. Gayatri Vineela et al. [16] performed an experiment in which the ultimate tensile strength of hybrid short fiber composites comprised of glass fiber, carbon fiber, and epoxy resin is predicted using artificial neural network approaches. It was discovered that ANN can predict the values of tensile strength more precisely than the regression model. Mishra et al. [17] conducted an experiment to demonstrate a MATLAB-based artificial neural network (ANN)-based approach for forecasting the deflection behavior of three kinds of

beams: plain, steel-reinforced, and bamboo-reinforced beams. The findings demonstrate that the ANN is a potent and trustworthy technique for evaluating the deflection behavior of concrete beams under the studied loading circumstances. Doblies et al. [18] have developed a model to predict the mechanical properties, as well as the thermal exposure time and temperature of epoxy resin, using Fourier-transform infrared spectroscopy (FTIR)-spectroscopy, data processing, and artificial neural networks. Turco et al. [19] developed two Artificial Neural Networks (ANNs) in order to forecast the compressive (ANN1) and tensile (ANN2) strengths of natural fiber-reinforced CEBs. The correlation coefficients (R-values) for ANN1 and ANN2 were 0.97 and 0.91, respectively, demonstrating the great accuracy of their generated tools.

Summarizing the literature survey shows that, there is significant literature on the mechanical property testing of thermally aged GFRP. Also, several predictive models using multi-parameter models, regression and ANN techniques have been developed with good accuracy. It is evident that on a macroscopic level, the physical and chemical mechanisms causing a change in GFRP properties are well understood. However, the mechanical property values reported by different researchers remain in a large scatter for thermally aged GFRP. The precise physical micro-phenomena and chemical reactions, as well as how they interact, are still being researched. Again, most of the predictive models in the literature depend on testing the material and predicting the output value based on the test input parameters. This is a time-consuming process that involves disassembly, sample preparation and destructive testing. It costs a lot of money for applications in aerospace, automobile, marine and similar industries. As such, a computational method to estimate the mechanical properties of thermally aged GFRP would be very beneficial for a highly competitive and operational industry like Aerospace. However, determining the current material state and retracing the mechanical and thermal histories continue to be difficult tasks [18]. Hence, there is a research gap in further mechanical property testing of thermally aged GFRP due to the variations in results reported by researchers. Moreover, a computational method to estimate the mechanical properties of thermally aged GFRP remains largely unaddressed.

This research focuses on the characterization of mechanical properties of thermally aged glass fiber epoxy composite below and beyond the glass transition temperature (Tg). Also, a novel predictive model was developed for estimating the mechanical properties of thermally aged glass fiber reinforced plastic (GFRP) composites. The predictive model developed in this research and its exact design is completely novel and it has not been studied yet by researchers as per the literature review and best knowledge of the author. This model has the potential to save time and money by avoiding disassembly, sample preparation and destructive testing of GFRP components especially in aerospace line maintenance applications.

2. Materials and Methods

2.1. Materials Used

Commercially available high silica ($SiO_2 \geq 96\%$) woven Glass fiber cloth of 1100 grams per square meter (GSM) weight was selected as the reinforcing element for preparing the GFRP composite material. This glass fiber cloth was purchased from Jiangnan Company and originated in Jiangsu, China. The glass fiber fabric has a thickness of 1.2 mm and a thread count of 15 for WEFT and 20 for WARP. The tensile of the woven glass fiber cloth is 86.95 MPa as per the manufacturer's specification. To create one composite slab, two layers of glass fibers were sliced into 325mm x 325mm squares. As the matrix material, Araldite AW 106 IN epoxy resin and HV 953 U hardener were used. According to the manufacturer's recommendations, a 100:80 weight ratio of resin and hardener was utilized. The viscosity

(cP) at 25°C is 50000 and 35000, respectively, while the specific gravities of the hardener and resin are 1.17 and 0.92, respectively.

As this study involves thermal aging, the elevated temperature properties of the reinforcement and the matrix were very important considerations. The glass fiber cloth can reportedly withstand operating temperatures of up to 1100°C and has a melting point of 1700°C, according to the manufacturer. The glass transition temperature (Tg) of the resin-hardener is 63°C. The Glass Transition Temperature (Tg) is one of the most important properties of any epoxy and is the temperature region where the polymer transitions from hard, glassy material to a soft, rubbery material. It is the temperature of interest for our study as our selected thermal aging temperature ranges below (50°C) and beyond (100°C, 150°C and 200°C) this temperature.

2.2. Methodology

The methodology used for this study involved 10 interrelated steps. The first 5 steps were part of the experimental work which dealt with fabrication and characterization of the GFRP. The other 5 steps were part of the computational work which dealt with predictive modeling. The step-by-step graphical methodology is shown in Figure 1 as follows.

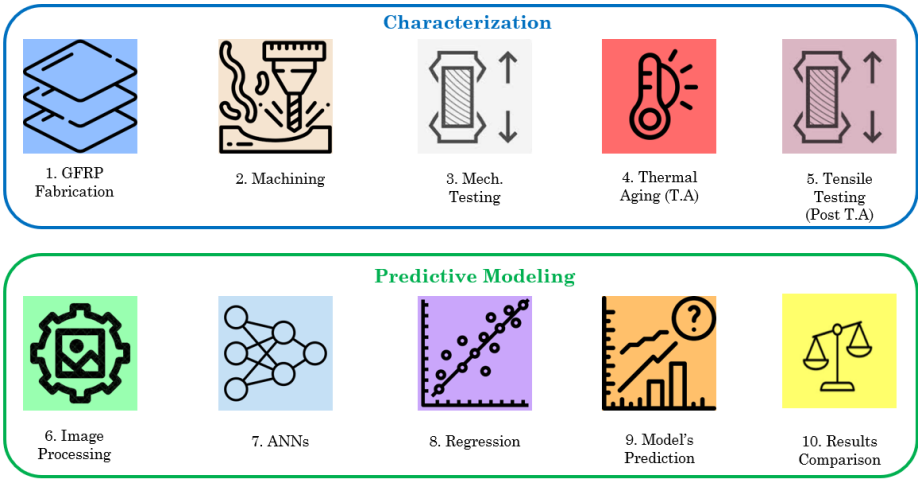

Fig. 1. Graphical methodology of this research

The details of the 10-step methodology are as follows:

- GFRP Composites were fabricated using woven and random glass fibers by hand-layup method.
- Samples for mechanical testing were prepared as per ASTM standards by mechanical cutting and laser cutting.
- These unaged samples underwent tensile test, flexural test, microhardness test and SEM imaging to find the effect of fiber orientation and machining on the mechanical properties.
- Tensile test Samples were thermally aged at different temperatures and times. Their distinct color changes at elevated temperatures were identified and photographed.
- Thermally aged Samples were mechanically tested as per ASTM standards and results including Ultimate Tensile Strength (UTS), Yield Strength, Maximum Strain, Elastic Modulus and Tangent Modulus were recorded.

- An image processing algorithm identified the color changes of the thermally aged samples (from the photos taken in step iv) and gave the most consistent Red, Green and Blue (RGB) color values as the output.
- Two ANNs were trained which took input of the RGB values and predicted the thermal aging variables (aging temperature and time) the samples underwent.
- A regression analysis was performed to correlate UTS and thermal aging variables (aging temperature and time).
- The ANN-predicted aging temperature and time were used to predict the UTS value using the regression equation developed in step viii. This was the final output of the predictive model.
- UTS from the experimental result (step v) and estimations of the predictive model (step ix) were analyzed and compared.

3. Experimental Work

3.1 Fabrication of GFRP Samples

The GFRP composite material was fabricated using the hand layup technique. A plywood mold with the dimensions of 325 mm × 325 mm x 10 mm was employed. A clear plastic release sheet was positioned at the bottom and coated with wax to make the removal procedure easier after production. To prevent air entrapment, the resin-hardener mixture was first placed in one layer and spread uniformly with a spatula. Then, one layer of the resin-hardener combination was put between two layers of glass fiber. The topmost layer was then filled with the resin-hardener combination and protected by a transparent plastic release film. Using a roller, gentle pressure was applied above the release film to release any trapped air. As soon as the topmost layer of resin-hardener was placed, the joint parts were clamped. The composite was then allowed to cure for 12 hours at room temperature under the weight of a 17 kg plywood sheet. The constructed composite slab had a 3mm thickness.

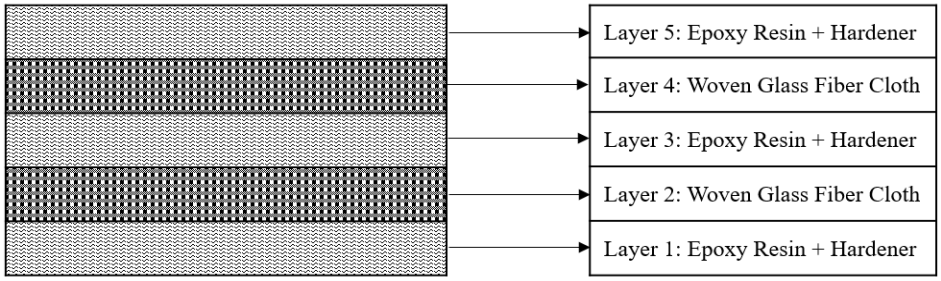

Fig 2. Arrangement of layers in fabricated GFRP composite

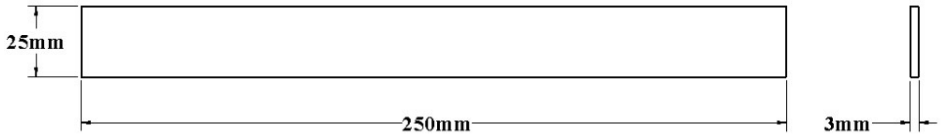

Fig 3. Solidworks drawing of tensile test sample

The configuration of the matrix and reinforcing layers of the manufactured glass fiber composite is depicted in Figure 2. Table 1 lists the components of the prepared composite

sample. The 325 mm × 325 mm x 3 mm composite slabs were mechanically cut and samples for mechanical testing were prepared. Bosch GWS 900-100 professional angle grinder with TJWELD 1.2 mm thickness cutting wheel was used to cut the samples. For tensile testing, samples were prepared as per ASTM D3039 standard. A total of 51 samples were prepared. The dimensions of the sample are shown in figure 3.

Table 1. Composition of the prepared composite sample

Material	Weight (gm)	Weight (%)
Glass Fiber Cloth	206	45
Epoxy Resin	138	30
Hardener	111	25
Total	456	100

3.2 Thermal Aging

Temperature and time were the two variables selected for the thermal aging of the samples. For thermal aging, specific temperatures and aging times were chosen considering the literature review and Tg of the epoxy. The selected thermal aging temperatures were 50°C, 100°C, 150°C and 200°C while the thermal aging time were 30 mins, 60 mins, 90 mins and 120 mins. The range of temperatures and aging time was selected based on the expected thermal conditions in Aerospace applications. Such temperatures and exposure times are frequently encountered in case of UAV operations and Air-conditioning bleed ducts of commercial aircraft.

Table 2. Sample group numbers and associated thermal aging variables

Sample group number (SGN)	Aging temperature	Aging time	Number of samples in the group
1	Unaged	Unaged	3
2	50°C	30 mins	3
3	50°C	60 mins	3
4	50°C	90 mins	3
5	50°C	120 mins	3
6	100°C	30 mins	3
7	100°C	60 mins	3
8	100°C	90 mins	3
9	100°C	120 mins	3
10	150°C	30 mins	3
11	150°C	60 mins	3
12	150°C	90 mins	3
13	150°C	120 mins	3
14	200°C	30 mins	3
15	200°C	60 mins	3
16	200°C	90 mins	3
17	200°C	120 mins	3
Total number of samples			51

Tensile testing samples were thermally aged in Carbolite Gero CWF 13/13 furnace. As per the manufacturer's specifications, this furnace can reach the maximum temperature of 1300°C in 121 minutes with a maximum continuous operating temperature of 1200°C. For each one of the thermal aging temperatures, samples were aged at all the above aging times. As such total 16 combinations of thermal aging were performed in the ovens. With the addition of the unaged samples, the total number of combinations was 17. These 17 combinations are labeled as sample group numbers (SGN). Each of the sample groups had

3 samples making a total of 51 samples for 17 groups. The sample group numbers (SGN) and associated thermal aging variables are shown in table 2.

3.3 Tensile Test

In a tensile test, a sample is subjected to controlled tension till it reaches failure. The tensile test was done as per ASTM D3039 standard. The tensile test is performed in the universal testing machine (UTM) PLS100 with a crosshead speed of 5mm/min. The flat samples are fixed between the grips of each head of the testing machine. To have a better grip on the grips of the tensile testing machine, end tabs are provided at both ends of the samples. The grip is set up in such a way that the direction of force applied to the sample is coincident with the longitudinal axis of the sample.

The Tensile test was performed for a total of 51 samples from 17 SGNs with 3 samples in each SGN. At first, 03 thermally unaged samples underwent tensile testing. From the tensile test data, max strain (%), UTS (MPa), yield strength (MPa), elastic modulus (MPa) and tangent modulus (MPa) were calculated. Afterward, 48 thermally aged samples underwent tensile testing. The average values of the 3 samples in each group were considered for the respective group. Finally, a total of 17 sets of tensile test data was obtained including UTS, Max Strain and Yield Strength. The tensile test dataset with thermal aging variables and corresponding mechanical properties is shown in table 3.

Table 3. Tensile test dataset with thermal aging variables and corresponding mechanical properties

SGN	Temperature (°C)	Time (mins)	UTS (MPa)	Max Strain (%)	Yield Strength (MPa)
1	Unaged	Unaged	85.6	6.34	25.60
2	50	30	79.33	5.52	23.83
3	50	60	71.33	5.74	20.50
4	50	90	70.00	6.30	21.47
5	50	120	72.33	5.71	21.54
6	100	30	64.00	5.64	19.33
7	100	60	58.00	5.39	17.65
8	100	90	69.00	5.59	20.67
9	100	120	61.00	4.83	18.53
10	150	30	70.33	4.37	17.00
11	150	60	56.33	4.22	17.00
12	150	90	80.67	5.02	19.00
13	150	120	62.50	5.08	19.00
14	200	30	47.00	3.71	11.90
15	200	60	63.33	4.41	18.50
16	200	90	64.67	4.06	18.50
17	200	120	58.33	3.99	17.67

4. Predictive Model

This model uses image processing, regression analysis and cascaded artificial neural networks (ANN) which were developed earlier to predict the Ultimate Tensile Strength (UTS) value with a photographic image of the sample. The model can also be customized to predict any mechanical properties with visually distinguishable identifiers dependent on thermal aging.

This model uses the color changes due to thermal aging from the photographic image as an identifier. This identifier allows it to estimate the UTS value without destructive testing. Firstly, the Image processing program reads the photographic image of the thermally aged samples and calculates the RGB color values. Two cascaded ANNs are used to estimate the thermal aging variables from the RGB color values. ANNs are used because this estimation follows a data-driven approach rather than a mathematical formulation. It involves several variables like the lighting conditions of the photo, image noise and sample precleaning which can impact the data accuracy of RGB values. With such scattered data, ANNs are found to be useful. However, the larger the dataset, the better. The regression analysis develops a mathematical equation to estimate the UTS values from the thermal aging temperature and time. This dataset in table 3 from the experimental work is used for the regression analysis. To aid the visualization of data flow between the experimental work and the predictive model, a graphical methodology has been prepared and show in Figure 4.

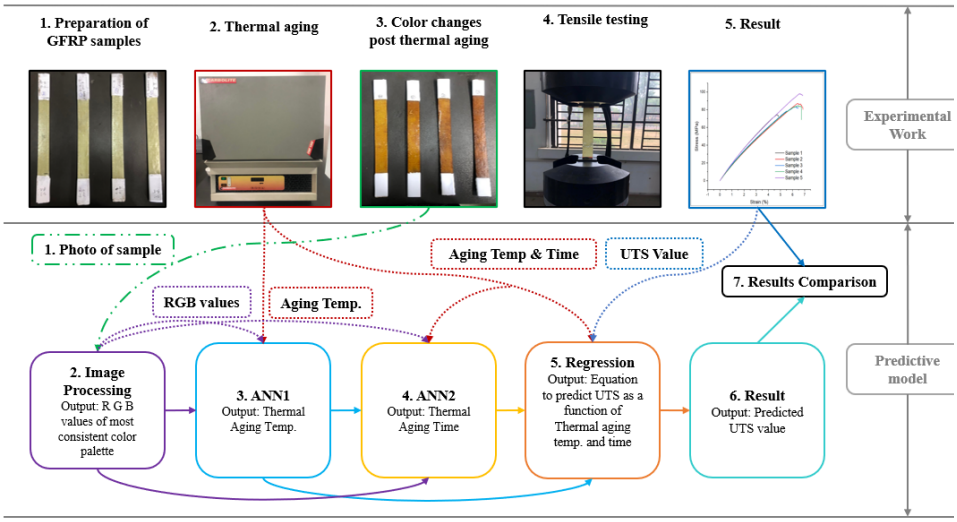

Fig. 4. Graphical methodology of the predictive model

The upper half of the figure shows the experimental work. The work process has been shown in 5 sequential steps starting from preparation of GFRP sample, thermal aging in the oven, color changes post thermal aging, tensile testing and results. Step no 2, 3 and 5 has been shown in red, green and blue color respectively. This is done to better distinguish the flow of data from these steps to the predictive model.

The lower half shows the predictive model. There are 7 sequential steps starting from the photo of the sample, image processing, ANN1, ANN2, regression, result and results comparison. 3 types of lines have been shown in the graphical methodology. Continuous lines indicate the operational phase of the predictive model. Dotted lines indicate the training phase of the predictive model. Step 1 is common for both the operational and training phase of the model. It is indicated by 'long dash dot dot' line.

4.1 Image Processing

After the thermal aging was done, it was noted that the samples were undergoing a color change at 150°C and 200°C. This started at 150°C with a very slight shade of brown color

which became more apparent at 200°C. Also, as the aging time increased, the shade of brown color became progressively darker. As such, this change of color could be used as an identifier to predict the thermal aging variables i.e., temperature and time.

To meet this purpose, A MATLAB image processing program was developed which can read and identify the color changes of the samples. SGN 10-17 were exposed to thermal aging at 150°C and 200°C. The photos of these SGN 10-17 were uploaded to the MATLAB program. To minimize the issues of lighting conditions, image noise and sample precleaning, all the samples were photographed in controlled environment with the same camera and lighting conditions. The program performed calculations and gave the most consistent value of the Red, Green and Blue color (RGB) values in a matrix form for each of the samples. The code was optimized in such a way that even if there was some slight variation of color throughout different areas of the sample, the code was able to figure out the most consistent value. The MATLAB pseudocode for the image processing algorithm is shown in Figure 5.

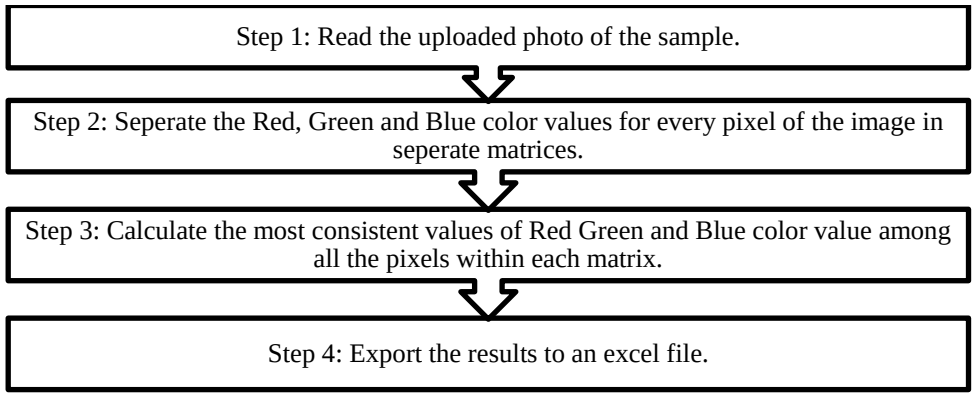

Fig. 5. MATLAB pseudocode of the image processing algorithm.

4.2 Artificial Neural Networks

Artificial Neural Networks (ANN) is a biologically-inspired computational method. It is one of many Artificial Intelligence algorithms and techniques. The ANN technique is based on a group of interconnected units or nodes called artificial neurons. The architecture of ANN consists of an input layer, one or several hidden layers and an output layer. As their name suggests, the input layer provides the input parameters to the ANN and the output layer provides the desired output. The calculations are performed by the hidden layers by means of weights and biases. The overall structure loosely models the neurons in a biological brain.

Using MATLAB, two ANNs are used in series to predict the thermal aging temperature and time. ANN1 takes 3 inputs as the RGB values and outputs the thermal aging temperature x_1. ANN2 takes 4 inputs including the same 3 previous RGB values and the output of the first ANN, x_1. The output of the second ANN is the thermal aging time x_2. Both ANNs consist of two layers including one hidden layer and one output layer. The hidden layer has 10 neurons and the output layer has 1 neuron. The transfer function of the hidden layer is chosen as tansigmoid while the transfer function of the output layer is chosen as purelin. Figure 6 shows the architecture of the two ANNs.

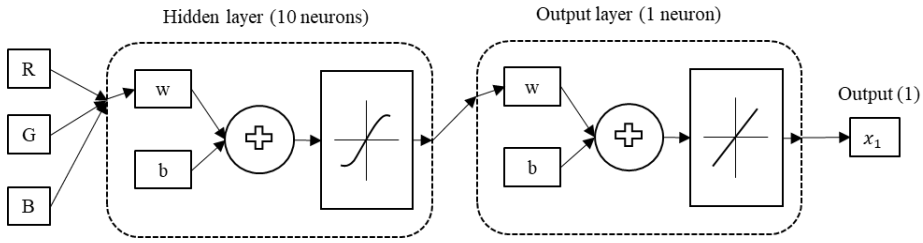

(a)

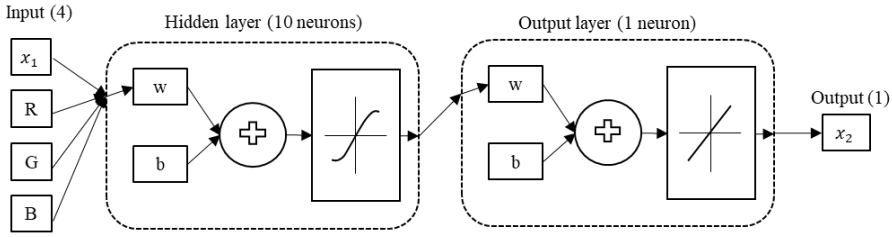

(b)

Fig. 6. The architecture of the two ANNs: (a) ANN1 (b) ANN2

Total 24 sets of thermal aging data were used for the training and testing of the two ANNs. Among the 24 sets, 19 set were used for the training and the remaining 5 sets were used for testing. Table 4 and Table 5 show the 19 sets of training data for ANN1 and ANN2 respectively.

Table 4. Training data for ANN1

	Input (3)			Output (1)
Dataset No	R	G	B	Aging Temp (x_1)
1	134	116	65	150
2	132	116	65	150
3	158	137	76	150
4	154	135	74	150
5	147	128	76	150
9	154	135	76	150
7	130	112	60	150
8	162	142	82	150
9	153	133	68	150
10	144	92	21	200
11	137	85	19	200
12	133	73	16	200
13	128	75	16	200
14	123	63	11	200
15	91	44	18	200
16	109	51	14	200
17	89	37	16	200
18	99	41	21	200
19	92	35	14	200

Table 5. Training data for ANN2

	Input (4)				Output (1)
Dataset No	R	G	B	Temp (x_1)	Aging Time (x_2)
1	134	116	65	150	30
2	132	116	65	150	30
3	158	137	76	150	60
4	154	135	74	150	60
5	147	128	76	150	90
9	154	135	76	150	90
7	130	112	60	150	90
8	162	142	82	150	120
9	153	133	68	150	120
10	144	92	21	200	30
11	137	85	19	200	30
12	133	73	16	200	60
13	128	75	16	200	60
14	123	63	11	200	60
15	91	44	18	200	90
16	109	51	14	200	90
17	89	37	16	200	90
18	99	41	21	200	120
19	92	35	14	200	120

The training performance of ANN1 and ANN2 are shown in figure 7 and figure 8 respectively.

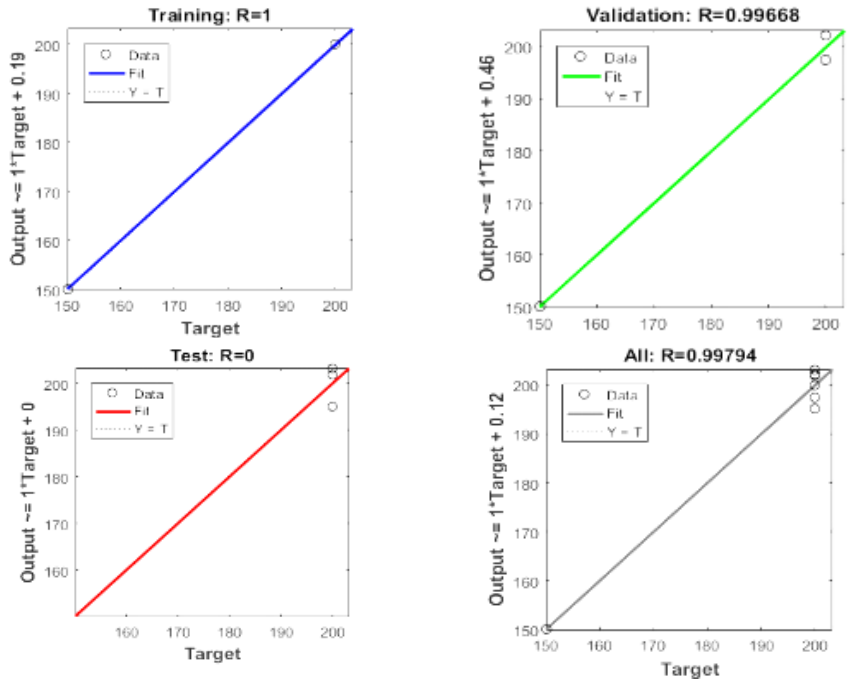

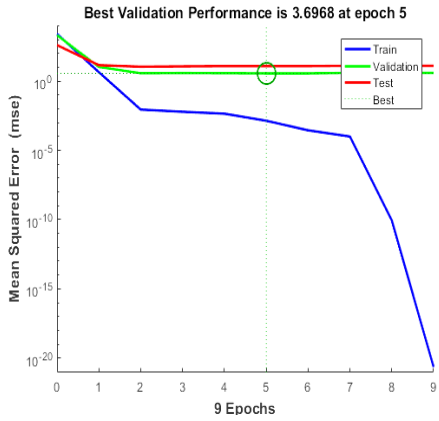

Fig. 7. Training performance of ANN1

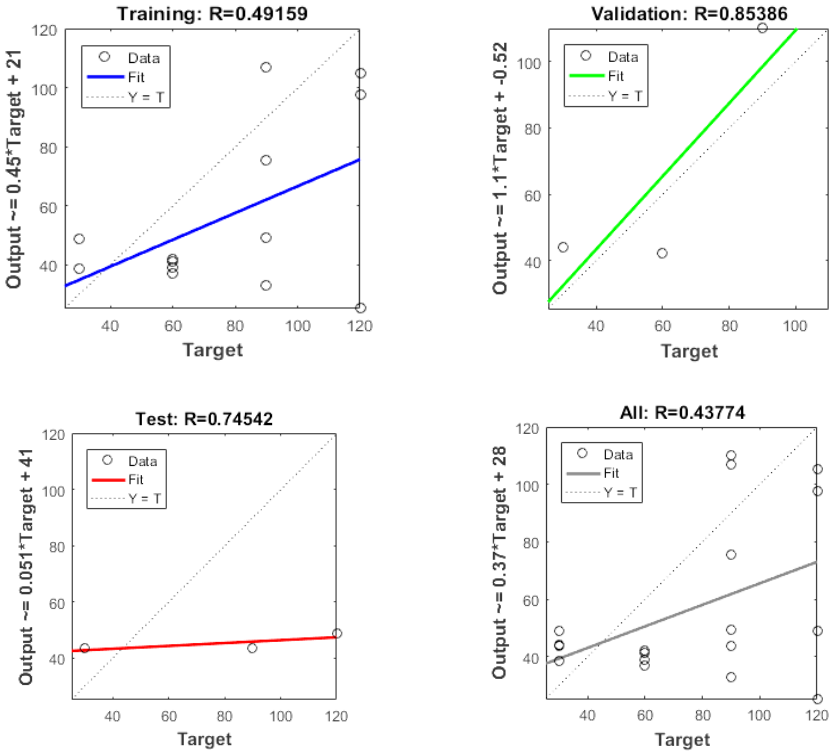

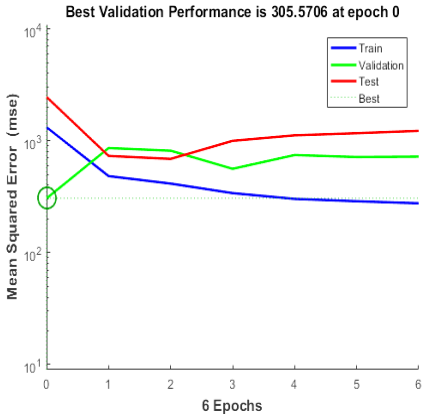

Fig 8. Training performance of ANN2

After the training of the ANNs are complete, they are tested with 5 sets of data. Table 6 and table 7 show the testing data for ANN1 and ANN2 respectively.

Table 6. Testing data for ANN1

Dataset No	Input (3) R	G	B	Output (1) Temp (x_1)
1	149	130	68	150
2	149	131	70	150
3	142	121	59	150
4	130	76	17	200
5	98	34	10	200

Table 7. Testing data for ANN2

Dataset No	Input (4) R	G	B	Temp (x_1)	Output (1) Aging Time (x_2)
1	149	130	68	150	30
2	149	131	70	150	60
3	142	121	59	150	120
4	130	76	17	200	30
5	98	34	10	200	120

4.3 Regression Analysis for UTS and Max Strain

A multi-regression analysis was performed in Minitab software. The regression analysis developed an equation to estimate the UTS values from the thermal aging variables. The thermal aging temperature and time were considered as the two independent variables. UTS was the dependent variable. The two cascaded ANNs estimated the thermal aging temperature and time, which were given as input to the developed regression equation.

The tensile testing dataset of SGN 1-17 shown in Table 3 was used to perform the regression. Figure 9 shows the regression model and its various parameters.

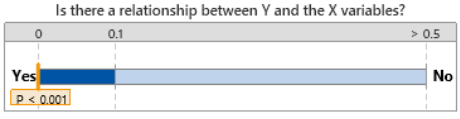

The relationship between Y and the X variables in the model is statistically significant (p < 0.10).

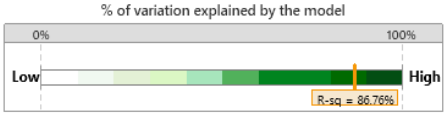

86.76% of the variation in Y can be explained by the regression model.

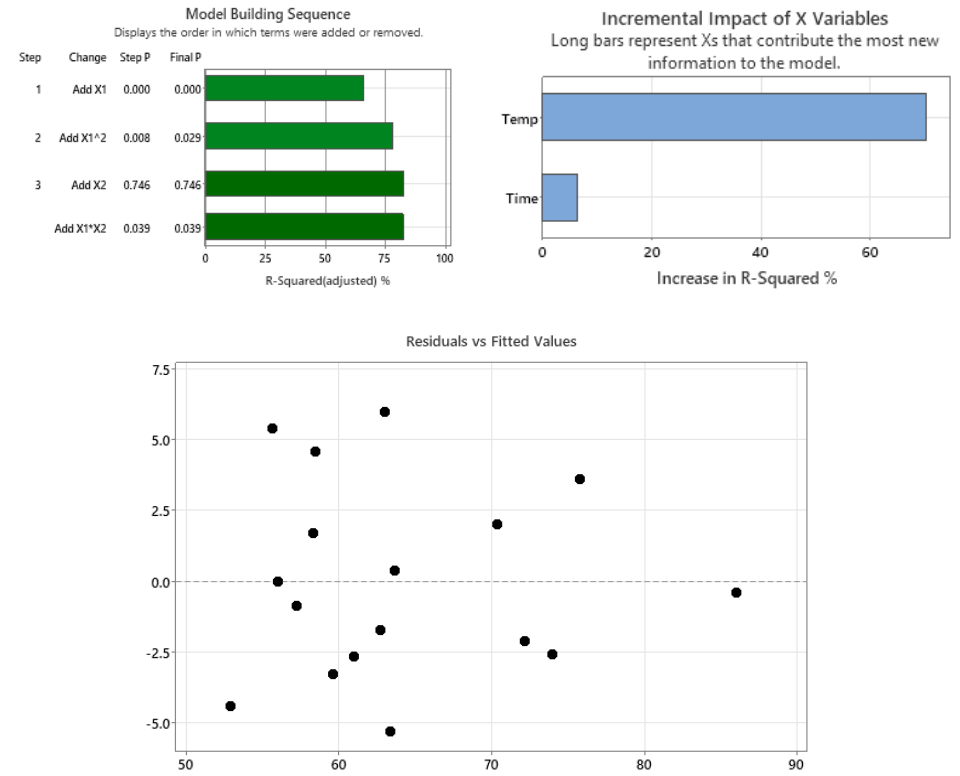

Fig. 9. The regression model and its various parameters

From the above figures, it is observed that the p-value of the regression model was less than 0.10 which indicates a strong relationship between the y and x variables. The R^2 value was 86.76% which means that 86.76% of the variation in y can be explained by the regression model. The R^2 adjusted value was found as 82.351% which indicates that most of the variables were useful in terms of generating the model. The incremental impact of x variables indicated that aging temperature had a 70.3987% impact on increasing R^2 value compared to only 6.57032% for aging time. Also, there were no residual values nor any strong curvature or clusters which would have indicated problems with the regression model. All the data points fall randomly on both sides of zero indicating a good fit.

The regression analysis found the relationship for UTS as:

$$y = 95.63 - 0.4070 \times x_1 - 0.1099 \times x_2 + 0.000900 \times x_1^2 + 0.000998 \times x_1 \times x_2 \quad (1)$$

Where, y = UTS (MPa), x_1 = Thermal aging temperature (°C) and x_2 = Thermal aging time (mins).

5. Results and Discussion

Results from the experimental work were analyzed to obtain insights about the mechanical properties of the GFRP. Also, the data from the experimental work was used to develop the predictive model. The following subsections describe the results and discussion of the experimental work and predictive model separately.

5.1. Experimental Work

Results and discussion of the experimental work are presented in this section. It is further divided into three subsections namely; Tensile Test of Unaged Samples, Thermal Aging and Tensile Test of Thermally Aged Samples.

5.1.1. Tensile Test of Unaged Samples

GFRP composites were fabricated and tensile testing samples were prepared as per ASTM D3039 standard. Figure 10 shows the mechanical properties of thermally aged GFRP samples.

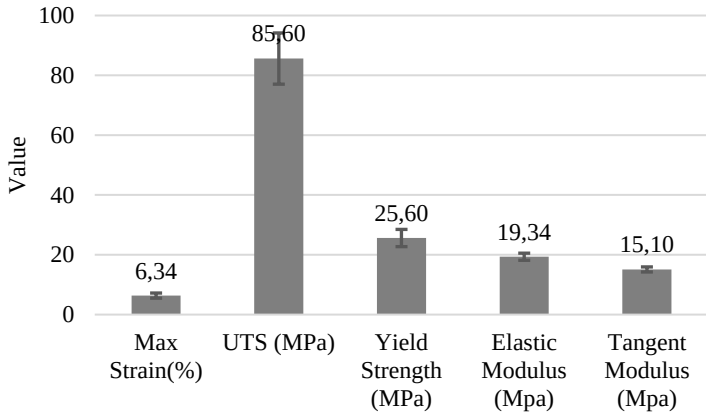

Fig. 10. Mechanical properties of thermally aged GFRP samples

From the figure, it is found that tensile testing of thermally unaged samples revealed mechanical properties UTS 85.60 MPa, Max Strain 6.34%, Yield Strength 25.60 MPa, Elastic Modulus 19.34 MPa and Tangent Modulus 15.10 MPa. It is to be noted that the UTS value of 85.60 MPa found by the tensile test is very close the UTS value of 86.95 MPa reported by the manufacturer of the glass fibers. Hence, it is apparent that during the tensile test, the glass fibers were the ultimate load-bearing member upon which the tensile strength of the GFRP was dependent.

5.1.2. Thermal Aging

During the thermal aging process at 100°C (SGN 6,7,8 and 9), very mild smoke and a burning smell were noticed. This smoke and smell effect became more noticeable at 150°C (SGN 10,11,12 and 13). At 200°C (SGN 14,15,16 and 17) the smoke and burning smell were clearly noticeable. This was expected as the glass transition temperature (Tg) of the epoxy is 63°C.

Also, at 150°C (SGN 10,11,12 and 13), the tensile test samples started to show color changes with the introduction of very slight shades of brown. At 200°C (SGN 14,15,16 and 17) this color change effect became apparent. In SGN 14, the color was light brown. As the thermal aging time increased, the brown color became progressively darker in SGN 15, 16 and 17. The color change effect due to thermal aging is shown in figure 11.

2, 3, 4 and 5 (SGN, Left to Right)

6, 7, 8 and 9 (SGN, Left to Right)

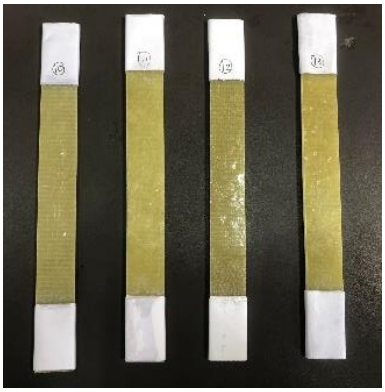

10, 11, 12 and 13 (SGN, Left to Right)

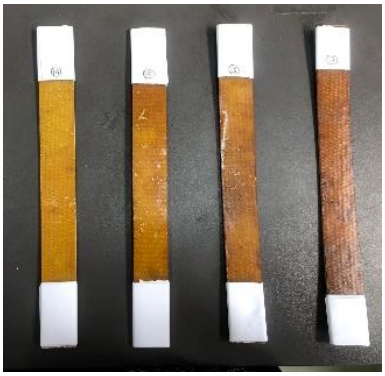

14, 15, 16 and 17 (SGN, Left to Right)

Fig 11. Color change effect due to thermal aging

The burning smell and color changes are mainly related to the oxidation process. Most notably; the carbonyl formation in the epoxy backbone due to thermo-oxidation is the cause for the color change of the material [20]. These findings agree with the existing literature. According to the literature, a higher temperature and longer exposure time typically result in a darker color. [12]. Although, the details are not fully understood yet [20], [21].

5.1.3. Tensile Test of Thermally Aged Samples.

In the present work, Ultimate Tensile Strength (UTS) is the mechanical property of interest. As such, it is analyzed with much deliberation. Figure 12 shows the change in UTS due to thermal aging. The Figure is divided into 5 separate graphs to aid the visualization of the thermal aging effect due to a fixed temperature and increasing aging time. Finally, graph 12 (e) shows the effect with all sample group numbers sequentially. The black bar in this graph represents the UTS value for unaged samples.

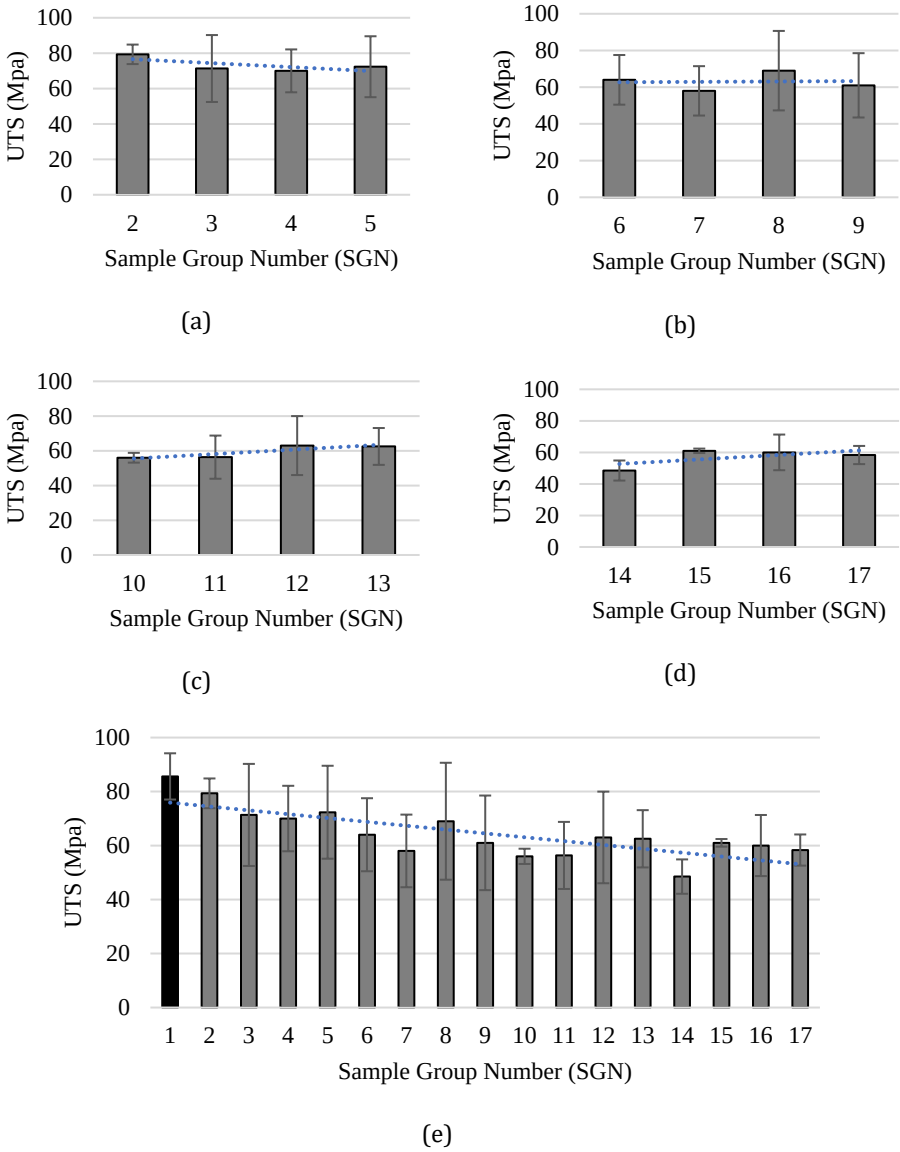

Fig. 12. Change of UTS due to thermal aging for different SGN

(a) SGN 2-5, (b) SGN 6-9, (c) SGN 10-13, (d) SGN 14-17 and (e) SGN 1-17

It is observed that for SGN 2-5 a decreasing UTS, a clear trend is observed. SGN 6-9 shows a more consistent rend with UTS values increase and decrease in an oscillating manner. For SGN 10-13 the UTS values slowly increase. For SGN 14-17, the UTS values increase initially but later reach a plateau. Finally, for graph 12(e) there is an overall trend of decreasing UTS is observed although there are noticeable variations as mentioned earlier. These variations in UTS due to different thermal aging are consistent with the literature. The initial decrease in UTS below and slightly over the Tg is expected due to the epoxy being rubbery and causing voids inside the material substrate. However, the increase in UTS at higher temperatures (SGN 11,12,13,15,16,17) is not fully understood by the author and requires further research.

Similar to UTS, Figure 13 shows the change of Max Strain due to thermal aging. The Figure is divided into 5 separate graphs to aid the visualization of the thermal aging effect due to a fixed temperature and increasing aging time. Finally, graph 13 (e) shows the effect with all sample group numbers sequentially. The black bar in this graph represents the Max Strain value for unaged samples.

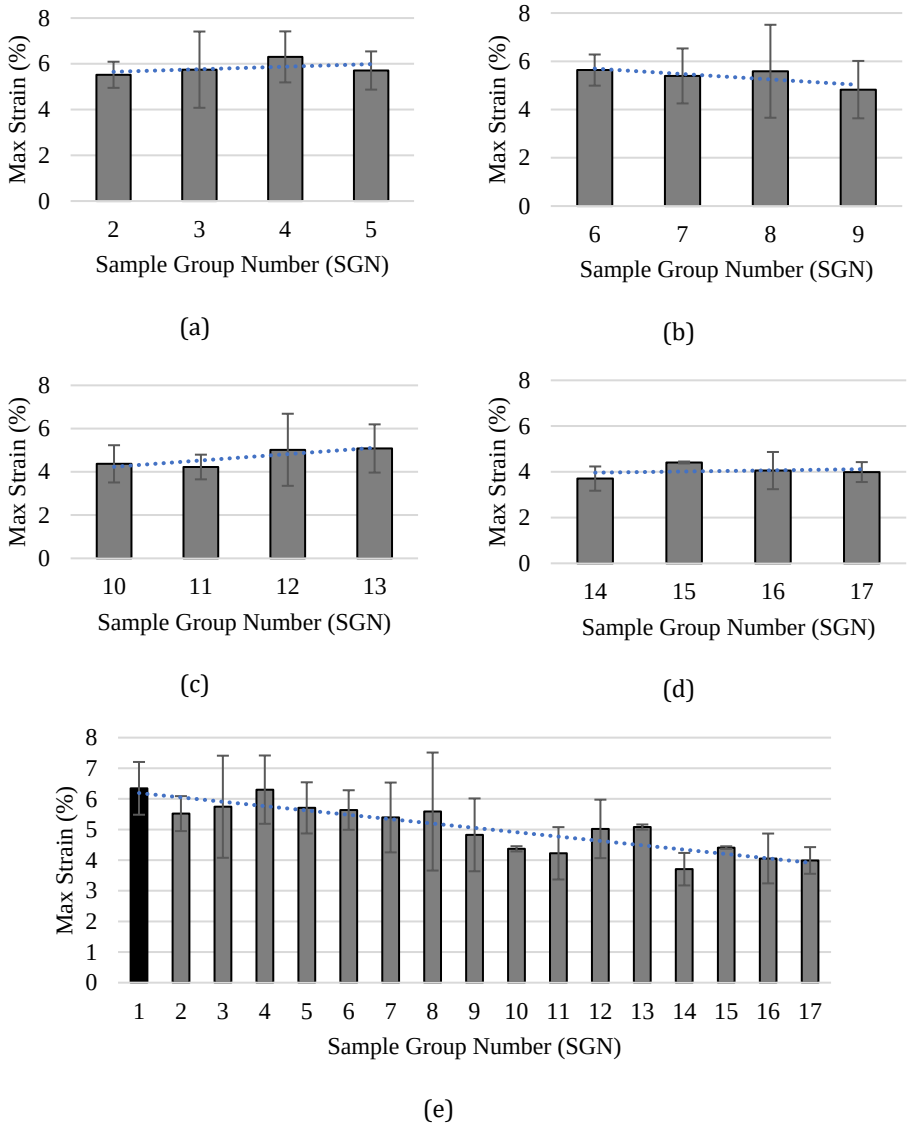

Fig. 13. Change of max strain (%) due to thermal aging for different SGN

(a) SGN 2-5, (b) SGN 6-9, (c) SGN 10-13, (d) SGN 14-17 and (e) SGN 1-17

Also, Figure 14 shows the change in Yield Strength due to thermal aging. The Figure is divided into 5 separate graphs to aid the visualization of the thermal aging effect due to a fixed temperature and increasing aging time. Finally, graph 14 (e) shows the effect with all sample group numbers sequentially. The black bar in this graph represents the Yield Strength value for unaged samples.

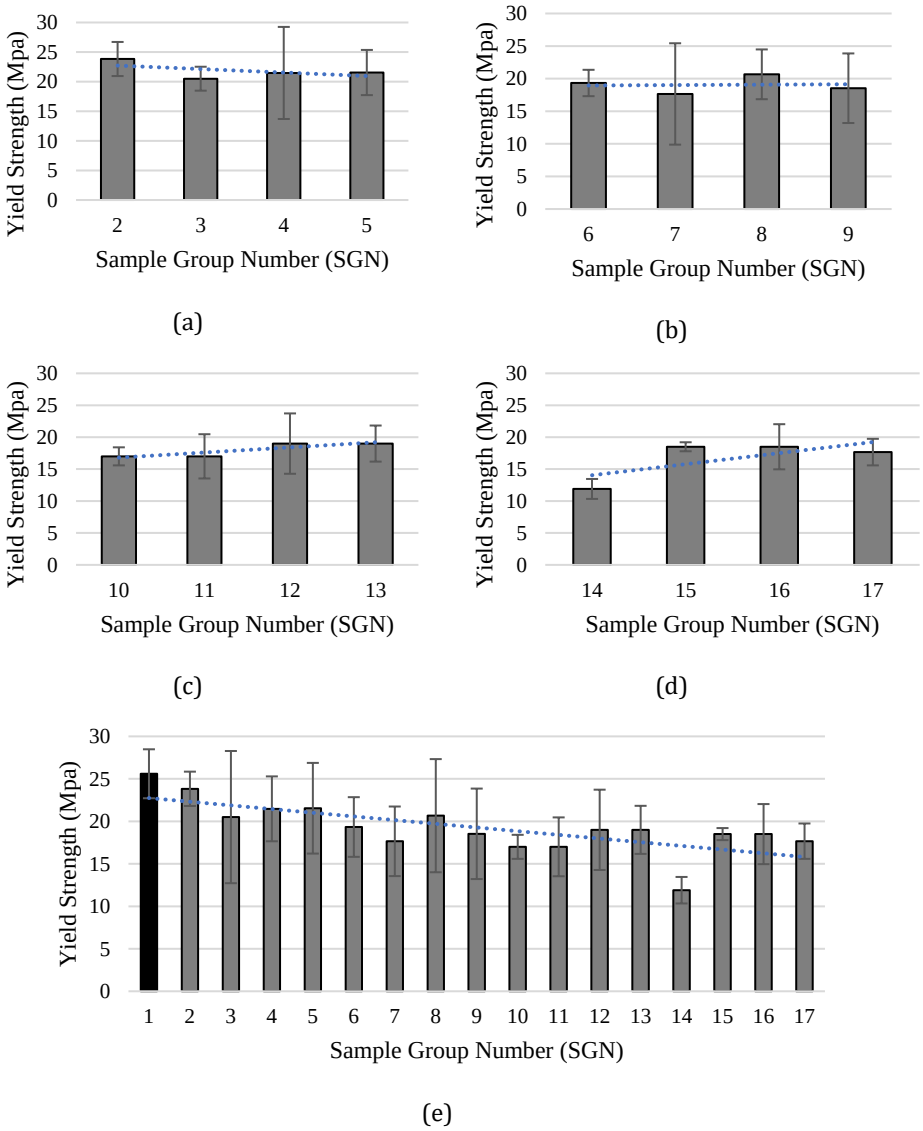

Fig. 14. Change of yield strength due to thermal aging for different SGN
(a) SGN 2-5, (b) SGN 6-9, (c) SGN 10-13, (d) SGN 14-17 and (e) SGN 1-1

As a general observation, from Figure 12 to 14, it is revealed that a gradual decrease in UTS, Max Strain and Yield strength values occurred as samples were exposed to increasingly higher temperatures during the thermal aging process. The highest value was obtained from the unaged samples while the lowest value was found from the thermally aged samples at 200°C 30 mins. The percentile decreases of UTS, Max Strain and Yield strength values were 43.34%, 41.48% and 53.52% respectively between the two extremes. The high amount of scattering in the mechanical properties after thermal aging is consistent with the literature [18].

Further analysis was performed to see variations in UTS of SGN 2 – 17, due to the variations in thermal aging temperature and time separately. Figure 15 shows the variation of UTS

due to thermal aging temperature and Figure 16 shows the variation of UTS due to thermal aging time.

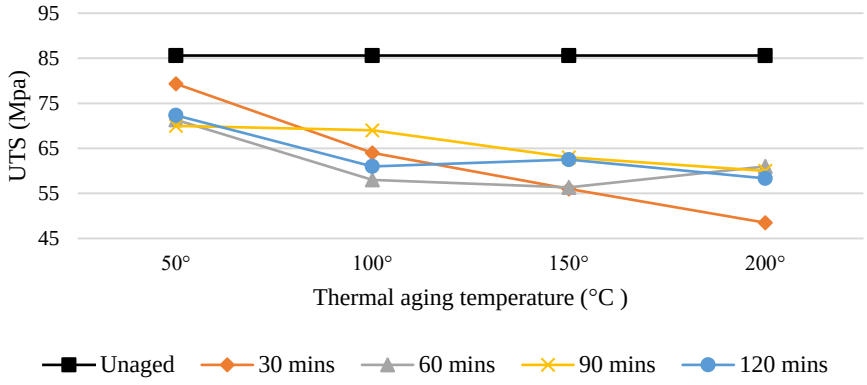

Fig. 15. Variation of UTS due to thermal aging temperature

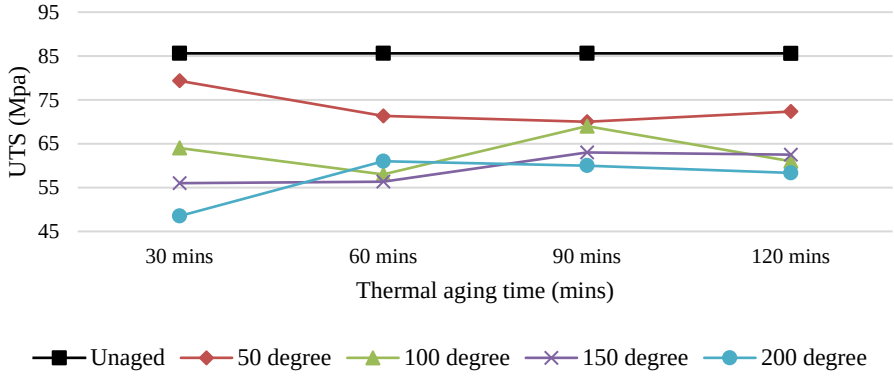

Fig 16. variation of UTS due to thermal aging time

From Figure 15, although there are some scatter and randomness in the mechanical properties after thermal aging consistent with the literature; the UTS of the thermally aged samples decreases as the thermal aging temperature increases. Generally, exposure to elevated temperatures and aging times causes the epoxy to be rubbery and develop voids inside the material substrate that lead to loss of strength [18]. However, from Figure 16, no specific trend is observed as the aging time increases for a specific temperature. In both cases, exposure to thermal aging always yields UTS values that are lower than the unaged UTS value.

Additionally, a Contour Surface plot was generated to understand the combined dependency of UTS of SGN 2 – 17 on thermal aging temperature and time. Figure 17 shows the contour plot of UTS.

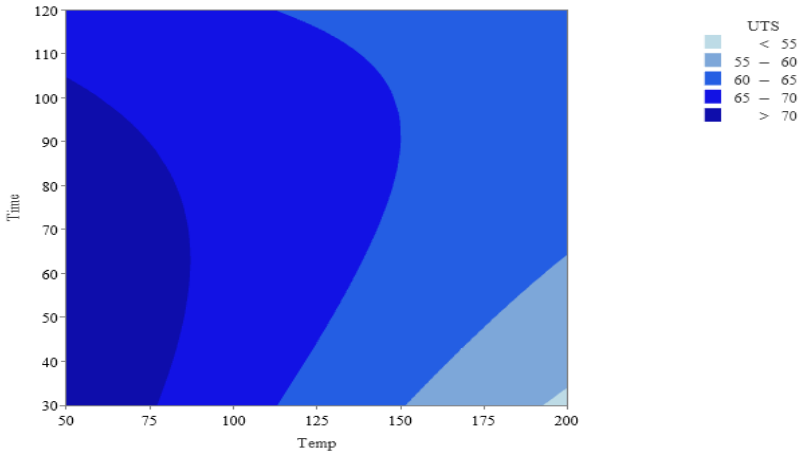

Fig 17. Contour plot of UTS

The contour plot shows the mapping of UTS values at various combinations of aging temperatures and time. In the plot, the UTS values are shown in 5 ranges which are represented by 5 shades of color. Darker shades represent higher values and lighter shades represent lower values. From the plot, the UTS decreases as temperatures reach higher values on the x-axis. However, as the aging time increases for a specific temperature in the y-axis, no trend is observed. It also affirms the previous findings that the sensitivity of UTS reduction is more dependent on the change of thermal aging temperature rather than the thermal aging time between 30 mins and 120 mins. However, existing literature suggests that a reduction of UTS can result in case of longer thermal exposures in similar temperatures [18].

5.2 The Predictive Model

Results and discussion of the predictive model are presented in this section. It is further divided into 4 subsections. In the first 3 subsections, the results and discussion of the Image processing, ANNs and Regression analysis have been presented. Finally, the performance and analysis of the complete predictive model have been presented in the fourth subsection.

5.2.1 Image Processing

The Image processing program calculated the most consistent Red Green and Blue color values of all 51 samples. Then the average of these values for 3 samples within each sample group was taken to obtain the Red Green and Blue color values for a particular sample group number. Figure 18 shows the Red Green and Blue color values for SGN 1-17.

From the above figure, it is observed that the RGB color values progressively decrease from SGN 1 to SGN 13. However, at SGN 14, when the thermal aging temperature reaches 200°C, the RGB color values decrease drastically. The overall trend of decreasing RGB color values is denoted by dotted lines for each respective color. The trend of decreasing RGB color values physically indicates the gradual darkening of color. This aligns with the observed gradually increasing brown color of the samples. Ultimately, the color reaches deep brown at SGN 17. This color change and the associated trend of RGB values agree with the color changes during thermal aging reported in Figure 11. These RGB values are used as an identifier for the ANNs.

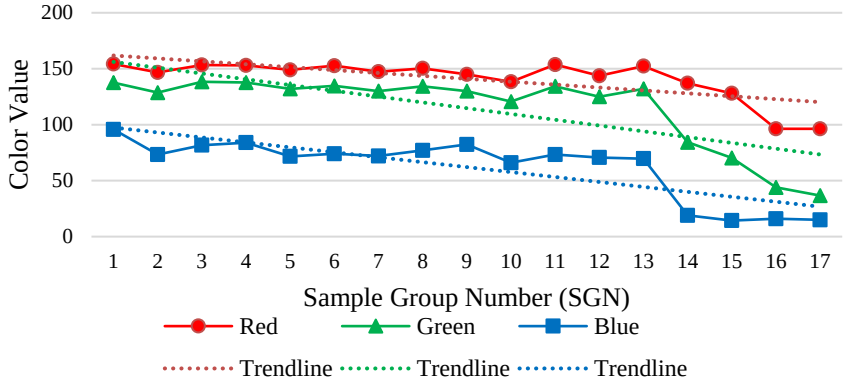

Fig. 18. Red Green and Blue color values for SGN 1-17

5.2.2. Artificial Neural Networks (ANNs)

The RGB values of the image processing program were given as input to the two cascaded ANNs to estimate the associated thermal aging temperature and time. The test performance of ANN1 and ANN2 are shown in Figure 19.

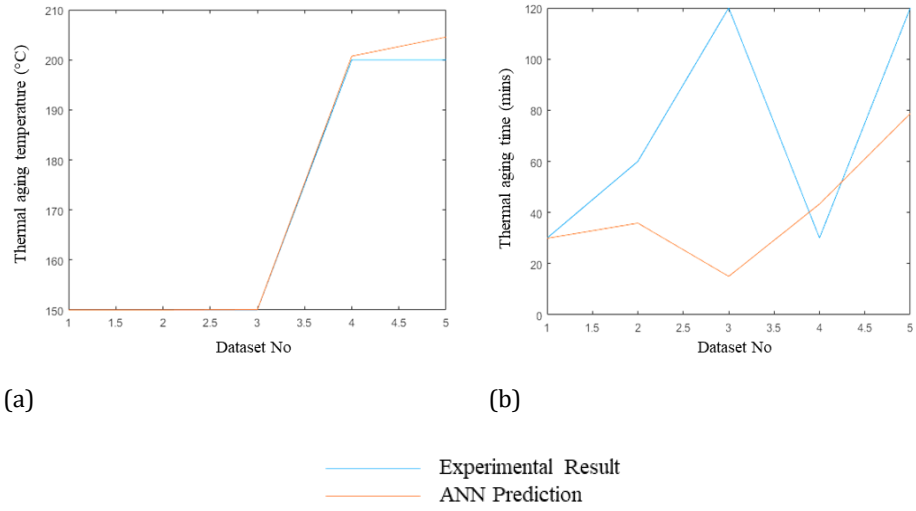

Fig 19. Testing performance of ANNs: (a) ANN1 (b) ANN2

From the above figure, it is noted that ANN1 made very accurate estimations compared to the experimental results. This is expected as per the findings and analysis of the experimental work in Figure 15. As there was a trend of declining UTS with increasing thermal aging time, ANN1 successfully followed the same. However, ANN2 predictions have high errors. This is also expected considering the experimental work in Figure 16. In this case, there were no clear trends which led to ANN2 making high errors. To achieve better results from ANN2, a much larger dataset is required,

5.2.3. Regression Analysis

A comparison was made between the results of the experimental work and the results obtained using the regression equation (1). Figure 20 shows the comparative plot of UTS values of SGN 1-17 obtained from experimental work and the regression equation.

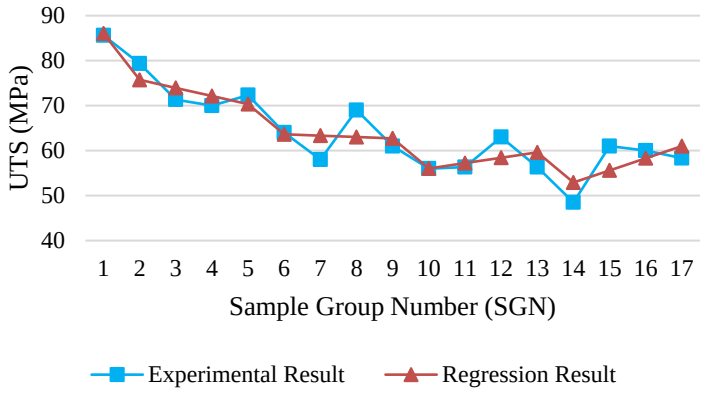

Fig. 20. Comparison of experimental and regression results for UTS

From the figure above it is seen that the UTS values obtained through the regression equation closely follow the experimental values. The average absolute error of all 17 SGN was calculated and found as 4%.

5.2.4. Performance of the predictive model

Combining the results from the Image Processing, Regression Analysis and Artificial Neural Networks; the predictive model predicted the UTS value of the thermally aged samples. The model was tested with 05 samples within SGN 10-17. Figure 21 graphically compares the experimental result and the predictive model predicted result. Table 8 shows the dataset of the experimental result and predictive model predicted result with associated errors.

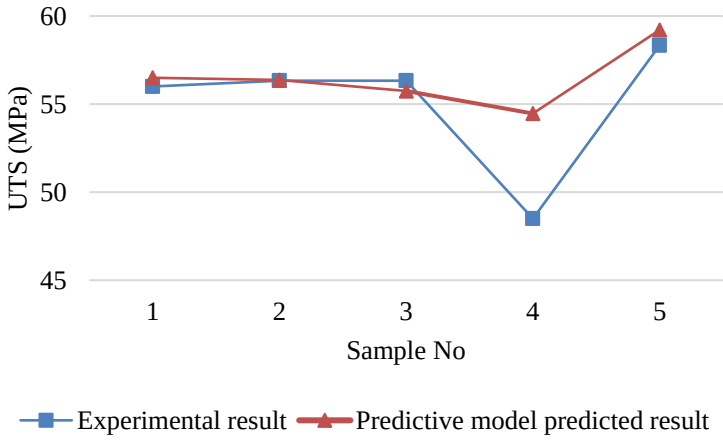

Fig. 21. Graphical comparison of experimental results and predictive model predicted results.

Table 8. The dataset of the experimental result and predictive model predicted results with associated errors.

Sample No	SGN	Temperature (°C)	Time (mins)	Experimental UTS (MPa)	Predictive Model predicted UTS (MPa)	Error (%)	Absolute Error (%)
1	10	150	30	56.00	56.50	-1%	1%
2	11	150	60	56.33	56.37	0%	0%
3	13	150	120	56.33	55.75	1%	1%
4	14	200	30	48.50	54.47	-12%	12%
5	17	200	120	58.33	59.21	-2%	2%
Average Absolute Error							3%

From the figure, it is evident that the predictive model estimated the experimental results of samples no 1, 2 and 3 with 99%, 100% and 99% accuracy. In sample no 4, the predictive model successfully followed the declining trend of the experimental result. However, the estimation had a 12% error. Again, in sample no 5, the predictive model successfully followed the rising trend of the experimental result and made an estimation with 98% accuracy. The average absolute accuracy of the predictive model is calculated as 97%.

The accuracy of the predictive model depends on the input image quality which influences the RGB values. Also, the accuracy largely depends on the regression equation as it is a best-fit equation by nature that inherently has some errors. Moreover, the predictive model is compared with experimental results which are also prone to scattering due to matrix rearrangement post-thermal aging, sample randomness and several other experimental factors.

It is seen that only in the case of sample 3, the predictive model made a noticeable error. This error may be attributed to the causes discussed above. In general, the accuracy of the predictive model can be maximized by increasing the number of experimental work samples and the ANN training dataset.

6. Conclusion

This study investigated the mechanical properties of thermally aged GFRP composites. Also, a novel predictive model was also developed consisting of image processing, regression analysis and cascaded artificial neural networks. Within the limitations of the study, the following conclusions can be made:

During thermal aging at 100°C, very mild smoke and a burning smell were noticed. This smoke and smell became more noticeable at higher temperatures. After thermal aging at 150°C, samples showed a very slight shade of brown color. At 200°C the samples became progressively dark brown as aging times increased. This gradual change of color is attributed to the oxidation process that occurs during thermal aging.

Tensile test results showed that compared to unaged samples, a general decreasing trend of UTS, Max Strain and Yield strength values were noted. However, when investigated for different ranges of temperatures separately, it became apparent that the different ranges of temperatures had fluctuations and scattering with different thermal aging times. This variation and scattering is consistent with the literature and may be attributed to several factors that require further study.

Further analysis of tensile test results reveals that, the UTS of the thermally aged samples gradually decreases as the thermal aging temperature increases up to 200°C. But no specific pattern is observed as the thermal aging time increases up to 120 mins. It is likely because the GFRP is tolerant of thermal aging time ranges selected for this study and hence did not produce any trend. A broader range of thermal aging time may be studied to explore this behavior further. However, in all cases, even the minimum exposure to thermal aging (50°C and 30 mins) reduced the UTS value below that of unaged samples. None of the thermally aged samples showed equal or higher UTS value than unaged samples.

The predictive model was developed by combining image processing, regression analysis and cascaded ANNs. The model estimated the UTS of the thermally aged GFRP with only the photographic image of the sample. The predictive model showed an average accuracy of 97% when compared to experimental results. With a sufficient dataset, this model can also be modified to predict any mechanical property that has color change as an identifier. This model has potential applications for non-destructive field testing of GFRP composites and can reduce operational costs.

Abbreviations

The following abbreviations are used in this manuscript:

ANN	Artificial Neural network
ASTM	American Society for Testing and Materials,
GFRP	Glass fiber reinforced plastics
RGB	Red, Green, Blue
SGN	Sample group number
UTS	Ultimate tensile strength

Reference

[1] Rao B SD, Sethi A, Das AK. Fiber laser processing of GFRP composites and multi - objective optimization of the process using response surface methodology. Journal of Composite Materials 2018;53:1459–73. https://doi.org/10.1177/0021998318805139

[2] Pavan G, Singh KK, Mahesh. Elevated thermal conditioning effect on flexural strength of GFRP laminates: An experimental and statistical approach. Materials Today Communications 2021;26:101809. https://doi.org/10.1016/j.mtcomm.2020.101809

[3] Erden S, Sever K, Seki Y, Sarikanat M. Enhancement of the mechanical properties of glass/polyester composites via matrix modification glass/polyester composite siloxane matrix modification. Fibers and Polymers 2010;11:732–7. https://doi.org/10.1007/s12221-010-0732-2

[4] Bakis CE, Bank LC, Brown VL, Cosenza E, Davalos JF, Lesko JJ, et al. Fiber-Reinforced Polymer Composites for Construction—State-of-the-Art Review. Journal of Composites for Construction 2002;6:73–87. https://doi.org/10.1061/(asce)1090-0268(2002)6:2(73)

[5] Bazli M, Ashrafi H, Jafari A, Zhao X-L, Gholipour H, Oskouei AV. Effect of thickness and reinforcement configuration on flexural and impact behaviour of GFRP laminates after exposure to elevated temperatures. Composites Part B: Engineering 2019;157:76–99. https://doi.org/10.1016/j.compositesb.2018.08.054

[6] GAO Kun, SHI Hanqiao, SUN Baogang, et al. Effects of hydro-thermal aging on properties of glass fiber/epoxy composites[J]. Acta Materiae Compositae Sinica, 2016, 33(6): 1147-1152. doi: 10.13801/j.cnki.fhclxb.20160108.001
[7] Zuo P, Tcharkhtchi A, Shirinbayan M, Fitoussi J, Bakir F. Effect of thermal aging on crystallization behaviors and dynamic mechanical properties of glass fiber reinforced polyphenylene sulfide (PPS/GF) composites. Journal of Polymer Research 2020;27. https://doi.org/10.1007/s10965-020-02051-2
[8] Birger S, Moshonov A, Kenig S. The effects of thermal and hygrothermal ageing on the failure mechanisms of graphite-fabric epoxy composites subjected to flexural loading. Composites 1989;20:341–8. https://doi.org/10.1016/0010-4361(89)90659-9
[9] Mouritz, A.P. Post-fire flexural properties of fibre-reinforced polyester, epoxy and phenolic composites. Journal of Materials Science 37, 1377–1386 (2002). https://doi.org/10.1023/A:1014520628915
[10] Dodds N, Gibson AG, Dewhurst D, Davies JM. Fire behaviour of composite laminates. Composites Part A: Applied Science and Manufacturing 2000;31:689–702. https://doi.org/10.1016/s1359-835x(00)00015-4
[11] Lan Z, Deng J, Song Y, Xu Z, Nie Y, Chen Y, et al. Color Changes and Mechanical Properties of Glass Fiber Reinforced Polycarbonate Composites after Thermal Aging. Polymers 2022;14:222. https://doi.org/10.3390/polym14020222
[12] Song Y, Deng J, Xu Z, Nie Y, Lan Z. Effect of Thermal Aging on Mechanical Properties and Color Difference of Glass Fiber/Polyetherimide (GF/PEI) Composites. Polymers 2021;14:67. https://doi.org/10.3390/polym14010067
[13] Zavatta N, Rondina F, Falaschetti MP, Donati L. Effect of Thermal Ageing on the Mechanical Strength of Carbon Fibre Reinforced Epoxy Composites. Polymers 2021;13:2006. https://doi.org/10.3390/polym13122006
[14] Gibson AG, Torres MEO, Browne TNA, Feih S, Mouritz AP. High temperature and fire behaviour of continuous glass fibre/polypropylene laminates. Composites Part A: Applied Science and Manufacturing 2010;41:1219–31. https://doi.org/10.1016/j.compositesa.2010.05.004
[15] Kim Y, Oh H. Comparison between Multiple Regression Analysis, Polynomial Regression Analysis, and an Artificial Neural Network for Tensile Strength Prediction of BFRP and GFRP. Materials 2021;14:4861. https://doi.org/10.3390/ma14174861
[16] Gayatri Vineela M, Dave A, Kiran Chaganti P. Artificial Neural Network based Prediction of Tensile Strength of Hybrid Composites. Materials Today: Proceedings 2018;5:19908–15. https://doi.org/10.1016/j.matpr.2018.06.356
[17] Mishra M, Agarwal A, Maity D. Neural-network-based approach to predict the deflection of plain, steel-reinforced, and bamboo-reinforced concrete beams from experimental data. SN Applied Sciences 2019;1. https://doi.org/10.1007/s42452-019-0622-1
[18] Doblies A, Boll B, Fiedler B. Prediction of Thermal Exposure and Mechanical Behavior of Epoxy Resin Using Artificial Neural Networks and Fourier Transform Infrared Spectroscopy. Polymers 2019;11:363. https://doi.org/10.3390/polym11020363
[19] Turco C, Funari MF, Teixeira E, Mateus R. Artificial Neural Networks to Predict the Mechanical Properties of Natural Fibre-Reinforced Compressed Earth Blocks (CEBs). Fibers 2021;9:78. https://doi.org/10.3390/fib9120078
[20] Krauklis A, Echtermeyer A. Mechanism of Yellowing: Carbonyl Formation during Hygrothermal Aging in a Common Amine Epoxy. Polymers 2018;10:1017. https://doi.org/10.3390/polym10091017
[21] Bellenger V, Verdu J. Oxidative skeleton breaking in epoxy–amine networks. Journal of Applied Polymer Science 1985;30:363–74. https://doi.org/10.1002/app.1985.070300132